Effect of Molecular Weight on the Phase Diagram and Thermal Properties of Poly(styrene)/8CB Mixtures

Farida Benmouna,[†,‡] Abdelylah Daoudi,[§] Frédérick Roussel,[§] Laurent Leclercq,[†] Jean-Marc Buisine,[§] Xavier Coqueret,[||] Mustapha Benmouna,[†,‡] Bernd Ewen,[†] and Ulrich Maschke*[,||]

Max-Planck-Institut für Polymerforschung, Postfach 3148, D-55021 Mainz, Germany; Laboratoire de Dynamique et Structure des Matériaux Moléculaires, Equipe de Thermophysique de la Matière Condensée - CNRS (UPRESA 8024), Université du Littoral, MREID, F-59140 Dunkerque, France; and Laboratoire de Chimie Macromoléculaire - CNRS (UPRESA 8009), Bâtiment C6, Université des Sciences et Technologies de Lille, F-59655 Villeneuve d'Ascq, France

Received July 26, 1999

ABSTRACT: Equilibrium phase diagrams and thermophysical properties of mixtures of poly(styrene) (PS) and 4-cyano-4′-*n*-octyl-biphenyl (8CB) are investigated. Three systems with widely different molecular weights of the polymer are considered in an attempt to assess the effects of the polymer size on the miscibility of PS and 8CB. The experimental phase diagrams are established using polarized optical microscopy (POM), light scattering (LS), and differential scanning calorimetry (DSC), and the results were analyzed with the predictions of the Flory−Huggins theory of isotropic mixing and the Maier−Saupe theory of nematic order generalized by McMillan to include smectic-A order. Good agreement is observed between theory and experiments. The solubility properties of mixtures with different polymer sizes are analyzed using the method suggested by Smith. The solubility limit of 8CB in PS is deduced from enthalpy changes at the nematic−isotropic transition temperature (T_{NI}) as a function of polymer molecular weight. It is found that the decrease of the solubility limit with increasing molecular weight is not linear and reaches a plateau value for higher molecular weights. The results obtained for the systems investigated here and for three other systems reported in the literature fall on a single master curve representing the solubility limit at T_{NI} as a function of polymer molecular weight.

1. Introduction

This paper deals with the equilibrium phase behavior and the thermophysical properties of mixtures of polystyrene (PS) and a low-molecular-weight liquid crystal (LMWLC) (4-cyano-4′-*n*-octyl-biphenyl or 8CB). Samples made of linear flexible chains with no mesogen groups and three different molecular weights dissolved in a low-molecular-weight LC are considered. This allows one to assess the effects of polymer size on the equilibrium phase behavior and thermal properties of polymer/LC mixtures. The LC 8CB exhibits in the bulk three distinct transitions and presents crystalline, smectic-A, and nematic phases.

Mixtures covering a wide range of compositions were prepared following the same procedure based on a combination of solvent-induced phase separation (SIPS) and thermally induced phase separation (TIPS).[1,2] Equilibrium phase behavior and thermophysical properties of these systems are the subject of growing interest because of the key role they play in a variety of practical applications such as digital displays, privacy windows, computers, TV screens, and so on.[1−4] Developing reliable and highly accurate methods to evaluate the content of LC dissolved in the polymer is crucial for determining the optimal operating conditions of devices made of such systems. It is clear that reduction of the amount of LC dissolved in the polymer matrix is not only an economic incentive to reduce the cost of these devices but also a goal sought to improve their operating conditions.[5,6] With regards to the thermophysical properties, the LC dissolved in the polymer acts generally as a plasticizer, reducing its glass-transition temperature, T_g.[7,8] Moreover, it affects strongly the refractive index matching condition between the polymer and the component of the LC perpendicular to its director. This condition is required to achieve maximum transmission of light when an electric field is applied.[9−11]

In the present work, we have chosen a model system made of well-characterized PS and a single-component LMWLC with well-defined transition temperatures including smectic A-nematic and nematic−isotropic transitions. Three PS samples covering a wide range of molecular weight and a very narrow molecular weight distribution were used. Under such conditions, we were able to characterize unambiguously the effect of polymer molecular weight on the phase diagram. To our knowledge, a similar experimental investigation was only reported by Kyu et al., who considered blends of poly(methyl methacrylate) and the eutectic LMWLC mixture known as E7 with a nematic−isotropic transition temperature of 60 °C.[12] The phase diagram and the phase-separation dynamics of PS (M_w = 218 000 g/mol) and E7 have been investigated by Kim and Kyu.[13]

In a recent paper,[14] preliminary data obtained by polarized optical microscopy (POM) and differential scanning calorimetry (DSC) of PS/8CB were given. These data were taken on a PS/8CB mixture where the polymer had a fixed molecular weight $M_w = 44 \times 10^3$ g/mol with a narrow distribution corresponding to $M_w/M_n = 1.05$. The experimental phase diagram was reported, and some thermophysical properties such as

* E-mail: maschke@univ-lille1.fr.
† Max-Planck-Institut für Polymerforschung.
‡ Permanent address: University Aboubakr Belkaïd of Tlemcen, Institute of Physics and Chemistry, Algeria.
§ Université du Littoral.
|| Université des Sciences et Technologies de Lille.

10.1021/ma991228d CCC: $19.00
Published on Web 01/19/2000

the glass-transition temperature and the fraction of LC in the nematic domains, α, were briefly described.

The present paper is an extension of the preceding one in several ways. First, two additional systems characterized by molecular weights of PS differing by orders of magnitude are considered. This allows one to assess unambiguously the effects of the polymer size on the equilibrium phase diagram and thermal properties of PS/8CB blends. By choosing widely different sizes, one hopes to reach conclusions representative of the whole range of polymer molecular weights from 4×10^3 to 200×10^3 g/mol. Unlike the results of Benmouna et al.,[14] the experimental data obtained here by POM, LS, and DSC are analyzed in more detail using a theoretical model that combines the Flory−Huggins[15] theory for isotropic mixing and the Maier−Saupe[16,17] theory for nematic order supplemented by the McMillan[18] extension to include the effects of smectic-A order. Changes in thermophysical properties resulting from changes in the polymer size are also considered. Enthalpy changes at the nematic−isotropic transition with LC composition yield valuable information on the solubility parameters and the amount of LC remaining in the polymer after the phase separation. New predictions on the solubility limit of the LC in different systems are made as a function of polymer molecular weight.

2. Theoretical Phase Diagram

The theoretical formalism that describes the phase behavior of mixtures of linear polymers and LMWLCs with smectic−nematic and nematic−isotropic transitions can be found in the literature.[19−27] A summary of this formalism is given in the present section. Valuable information is gained in the analysis of experimental data with regards to the effects of polymer size, transition temperatures, combined isotropic and anisotropic interactions, and so on. The general equations are given first before the explicit forms of free energies and chemical potentials and the procedure by which the equilibrium phase diagram is constructed.

2.1. General Equations. The starting free energy density for the systems under consideration here is a sum of two terms

$$f = f^{(i)} + f^{(a)} \tag{1}$$

The letter f represents a free energy density, and the superscripts (i) and (a) stand for isotropic and anisotropic, respectively. For the entire system containing a total number of N_t molecules, the total free energy is $F = N_t f$, with $N_t = N_1 n_1 + N_2 n_2$, with N_k and n_k being the degree of polymerization and the number of molecules per unit volume of species k, respectively, with $k = 1$ for the LC and $k = 2$ for the polymer. Similarly, we have $F^{(i)} = N_t f^{(i)}$ and $F^{(a)} = N_t f^{(a)}$. Knowledge of the free energy allows the calculation of the chemical potentials that, in turn, are used to determine the composition of phases in equilibrium. These are given by the derivatives

$$\mu_1 = \left(\frac{\partial F}{\partial n_1}\right)_{n_2,T,P} \qquad \mu_2 = \left(\frac{\partial F}{\partial n_2}\right)_{n_1,T,P} \tag{2}$$

where P and T represent pressure and temperature, respectively, and the quantities in the subscripts remain constant in the derivation. Sometimes, it is more convenient to write the chemical potentials in terms of derivatives with respect to volume fractions, $\varphi_1 = n_1 N_1 / N_t$ and $\varphi_2 = n_2 N_2 / N_t$. It will be assumed that all segments occupy the same volume and the mixture is incompressible, implying $\varphi_2 = 1\text{-}\varphi_1$. One finds

$$\frac{\mu_1}{N_1} = f - \varphi_2 \frac{\partial f}{\partial \varphi_2} \tag{3}$$

$$\frac{\mu_2}{N_2} = f - \varphi_1 \frac{\partial f}{\partial \varphi_1} \tag{4}$$

If two phases designated by single and double primes are in equilibrium, their compositions are given by the standard equations

$$\mu'_1 = \mu''_1; \qquad \mu'_2 = \mu''_2 \tag{5}$$

which are written explicitly as follows

$$f - \varphi_1 \frac{\partial f}{\partial \varphi_1}\Big|' = f - \varphi_1 \frac{\partial f}{\partial \varphi_1}\Big|'' \tag{6}$$

$$\frac{\partial f}{\partial \varphi_1}\Big|' = \frac{\partial f}{\partial \varphi_1}\Big|'' \tag{7}$$

The same relationships hold for isotropic, anisotropic, and total free energies. The choice of any of these contributions depends on the nature of phases in equilibrium. These general formulas are useful in the construction of the phase diagram. Their application to the systems under consideration here is based on a combination of the Flory−Huggins theory of isotropic mixing and the Maier−Saupe−McMillan theory of nematic and smectic orders, as we will discuss in the following sections.

2.2. Flory−Huggins Theory of Isotropic Mixing. The Flory−Huggins free energy density for a binary mixture is well-known

$$\frac{f^{(i)}}{k_B T} = \frac{\varphi_1}{N_1} \ln \varphi_1 + \frac{\varphi_2}{N_2} \ln \varphi_2 + \chi \varphi_1 \varphi_2 \tag{8}$$

where k_B is the Boltzmann constant and χ is the Flory−Huggins interaction parameter. Substituting eq 8 into eqs 3 and 4 yields

$$\frac{\mu_1^{(i)}}{k_B T} = \ln \varphi_1 + \left(1 - \frac{N_1}{N_2}\right)\varphi_2 + \chi N_1 \varphi_2^2 \tag{9}$$

$$\frac{\mu_2^{(i)}}{k_B T} = \ln \varphi_2 + \left(1 - \frac{N_2}{N_1}\right)\varphi_1 + \chi N_2 \varphi_1^2 \tag{10}$$

Likewise, the derivation of the isotropic free energy with respect to φ_1 is straightforward. Assuming that χ is independent of composition yields

$$\frac{\partial f^{(i)}}{\partial \varphi_1} = \frac{\ln \varphi_1 + 1}{N_1} - \frac{\ln \varphi_2 + 1}{N_2} + \chi(\varphi_2 - \varphi_1) \tag{11}$$

These results are sufficient to describe the isotropic phase behavior of the mixture. One needs only to specify the variation of χ with temperature. The following form is adopted here

$$\chi = A + \frac{B}{T} \tag{12}$$

where A and B are constants independent of T. They are chosen to obtain the best fit with the experimental data in the part of the diagram where the isotropic interaction is most significant.

2.3. Maier−Saupe−McMillan Theory of Nematic and Smectic-A Orders. The anisotropic free energy is obtained from the Maier−Saupe theory of nematic order generalized by McMillan to include smectic-A order.[19−27] Therefore, two order parameters are needed: the nematic order parameter s describes the orientation distribution defined by the angle θ between the LC director and a reference axis $0z$

$$s = \frac{1}{2}[3\langle\cos^2\theta\rangle - 1] \tag{13}$$

The smectic-A order parameter σ describes ordering along the $0z$-direction

$$\sigma = \frac{1}{2}\left\langle(3\cos^2\theta - 1)\cos\frac{2\pi z}{d}\right\rangle \tag{14}$$

The symbols $\langle ... \rangle$ denote averages with respect to the distribution of angle θ and coordinate z (along the direction of the smectic order), and d is the distance between consecutive smectic layers. The function $g(z, \mu)$ represents the distribution of director orientations

$$g(z, \mu) = \frac{\exp[-(u_n + u_s)/k_BT]}{4\pi Z} \tag{15}$$

where $\mu = \cos\theta$; u_n and u_s are the mean field potentials for nematic and smectic interactions. They are expressed in terms of mean field parameters m_n and m_s as follows

$$\frac{u_n}{k_BT} = -\frac{m_n}{2}(3\mu^2 - 1) \tag{16}$$

$$\frac{u_s}{k_BT} = -\frac{m_s}{2}(3\mu^2 - 1)\cos^2\frac{2\pi z}{d} \tag{17}$$

The capital letter Z represents the partition function and is related to the nematic and smectic orders

$$Z = \int\int d\mu\, dz \exp\left[\frac{m_n}{2}(3\mu^2 - 1)\right] \exp\left[\frac{m_s}{2}(3\mu^2 - 1)\cos 2\pi\frac{z}{d}\right] \tag{18}$$

The anisotropic free energy is given in terms of the distribution function

$$\frac{f^{(a)}}{k_BT} = \frac{F^{(a)}}{n_0k_BT} = \frac{\varphi_1}{N_1}\left\{\int\int g(z, \mu)\ln[4\pi g(z, \mu)]\, d\mu\, dz - \frac{1}{2}\nu\varphi_1(s^2 + \alpha\sigma^2)\right\} \tag{19}$$

The first term on the right-hand side of eq 19 is the entropy cost due to nematic/smectic orders, and the second term is an energy contribution. The integral defining the entropy can be reduced as

$$\int\int d\mu\, dz\, g(z, \mu)\ln[4\pi g(z, \mu)] = \ln Z - m_n s - m_s\sigma \tag{20}$$

Minimization of the free energy with respect to the two-order parameters (i.e., $\partial f^{(a)}/\partial s = 0$ and $\partial f^{(a)}/\partial\sigma = 0$ yields the mean field parameters m_n and m_s in terms of the order parameters s and σ

$$m_n = \nu s\varphi_1 \qquad m_s = \zeta\nu\sigma\varphi_1 \tag{21}$$

Combining eqs 19 to 21 yield the anisotropic free energy

$$\frac{f^{(a)}}{k_BT} = \frac{\varphi_1}{N_1}\left[-\ln Z + \frac{1}{2}\nu\varphi_1(s^2 + \zeta\sigma^2)\right] \tag{22}$$

where ν represents the quadrupole interaction parameter in the Maier−Saupe theory and ζ is the strength of smectic interaction in the McMillan model. The former is given by $\nu = 4.54T_{NI}/T$ while ζ depends on the ratio T_{SN}/T_{NI}. According to the theory of McMillan, and for the system under consideration here where $T_{SN}/T_{NI} = 0.98$, the parameter ζ will be given the value $\zeta = 0.9375$.

The anisotropic chemical potentials are obtained by a straightforward derivation of eq 22 using eqs 3 and 4. The results are

$$\frac{\mu_1^{(a)}}{k_BT} = -\ln Z + \frac{1}{2}(s^2 + \zeta\sigma^2)\nu\varphi_1^2 \tag{23}$$

$$\frac{\mu_2^{(a)}}{k_BT} = \frac{1}{2}\frac{N_2}{N_1}(s^2 + \zeta\sigma^2)\nu\varphi_1^2 \tag{24}$$

The above formalism is sufficient to construct the theoretical phase diagrams by a proper choice of the parameters characterizing the PS/8CB mixtures, as we shall see in the following sections of this paper.

3. Experimental Section

3.1. Sample Description. PS samples of different molecular weights were purchased from Aldrich (Saint Quentin Fallavier, France) and were used without purification. The molecular weights and their distributions were obtained by GPC calibrated with standard PS samples. These measurements were performed in tetrahydrofuran (THF) at room temperature and led to (a) $M_w = 4 \times 10^3$ g/mol, $M_w/M_n = 1.06$; (b) $M_w = 44 \times 10^3$ g/mol, $M_w/M_n = 1.05$; and (c) $M_w = 200 \times 10^3$ g/mol, $M_w/M_n = 1.09$.

The LC is 8CB showing a smectic-A order. It was purchased from Frinton Laboratories (New Jersey) and presents in the pure state characteristic transition temperatures that were provided by the manufacturer as follows: $T_{KS} = 21.5$ °C, $T_{SN} = 33.5$ °C, and $T_{NI} = 40.5$ °C.

3.2. Sample Preparation. PS and 8CB with different LC compositions were dissolved in THF at 50 wt % (weight percent). Mixtures were stirred mechanically for 12 h. Samples were prepared following the standard procedure for microscopy observations. A small amount of the mixture was cast on a clean glass slide, and the sample was left for 24 h to allow for a complete evaporation of the solvent. Another glass slide was put on top of the first one, and the dry sample was sandwiched between the two glass slides. The same procedure is repeated to have two or more samples at the same composition prepared independently to check for reproducibility of the results. Samples with the pure components were also obtained following a similar procedure, and it is worth noting that the same results were obtained as in the case of the pure components prepared without use of an organic solvent. For the DSC measurements, the samples were prepared by introducing

approximately 3 mg of the initial mixture into aluminum DSC pans prior to solvent evaporation.

3.3. DSC Measurements. DSC measurements were performed on an apparatus of the type SEIKO DSC 220C that was equipped with a liquid nitrogen system and allowed for cooling and heating ramps. The apparatus cell was purged with nitrogen at a rate of 50 mL/min. The same heating−cooling ramps were used for the microscopy measurements in the temperature range spanning from 20 to 70 °C. Data were recorded systematically on the second heating ramp.

Enthalpy changes at the nematic−isotropic transition denoted ΔH_{NI} and in the smectic−nematic transition denoted ΔH_{SN} are given in joule per gram of the sample. Uncertainties in these measurements were approximately ±0.05 J/g.

3.4. Polarized Optical Microscope (POM) Measurements. The POM used in this study is of type Leica DMRXP, equipped with a heating−cooling stage Linkam THMSE 600. Samples were heated at the rate 2 °C/min from room temperature to 15 degrees above the transition temperature leading to the isotropic phase. Then, samples were left for approximately 5 min in the isotropic state. Afterwards, the samples corresponding to 50 wt % 8CB or higher were cooled to room temperature at a rate of −2 °C/min. For the other samples with low concentration in LC, cooling was performed to $T = -10$ °C to allow for phase separation and formation of ordered regions if a LC phase does exist. This procedure is followed after 5 min by a heating ramp at a rate of 2 °C/min. Transition temperatures were recorded during the heating ramp.

3.5. Light Scattering (LS) Measurements. LS measurements were performed using the classical setup illustrated in Figure 1 from Leclercq et al.[28] The He−Ne Laser ($\lambda = 632.8$ nm) was polarized linearly, perpendicular to the scattering plane. The scattered intensity was measured in the VV mode (I_{vv}), where the analyzer axis is parallel to the polarization direction of the incident beam. The scattering pattern was recorded by a CCD camera. No anisotropic effects were found on the intensity pattern, allowing us to perform radial averages of the scattered intensity. The samples already used for POM measurements were submitted to the same heating/cooling cycle as that described in the previous section. In the isotropic state at temperatures above 70 °C, the scattering intensity was constant and exhibited low values. The temperature at which the scattering intensity undergoes a sharp or discontinuous increase was taken as the onset of phase separation.

4. Results and Discussions

4.1. Order Parameters and Phase Diagrams. *(a) Order Parameters.* Prior to the discussion of the phase diagrams, it would be useful to understand first the dependence of the order parameters on temperature and composition. The relative contribution of the anisotropic free energy to the total free energy and hence the existence of ordered domains in the phase diagram are related to the values of the order parameters. In view of the importance of these quantities, we represent in Figure 1 the variation of s and σ as a function of φ_1 for three temperatures. Thick and dashed curves represent s and σ, respectively. s undergoes two discontinuities at φ_{SN} and φ_{NI}, and exhibits two branches. The anisotropic free energy is nonzero only if the parameters s and σ are higher than the limiting values s_c and σ_c. Above the smectic-nematic transition temperature ($T_{SN} = 33.5$ °C) and below the volume fraction $\varphi_{SN} = T/T_{SN}$, there is no smectic order and σ is zero. Above the nematic isotropic−transition temperature ($T_{NI} = 40.5$ °C) and below $\varphi_{NI} = T/T_{NI}$, there is no nematic order. Below this composition, the smectic order disappears because σ becomes 0, and the nematic order remains alone until the composition reaches the composition φ_{NI}. The upper branch of the nematic order parameter is

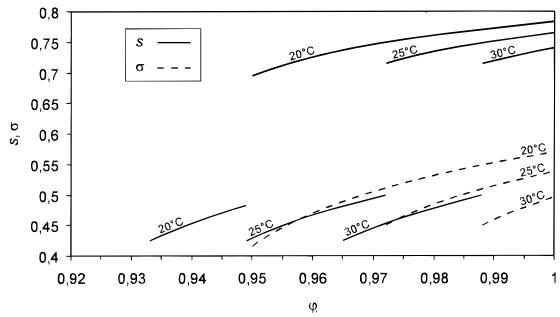

Figure 1. Variations of nematic s and smectic σ order parameters versus LC composition at three temperatures. The following quantities were used in this plot: $T_{SN} = 33.5$ °C, $T_{NI} = 40.5$ °C, and $\zeta = 0.9375$.

quite high due to the enhanced nematic order resulting from the emergence of the smectic-A order. The increase of the order parameter s in the presence of smectic interactions depends on the coupling parameter α that, in turn, is a function of the ratio T_{SN}/T_{NI}. For the present PS/8CB system, considering the values of T_{NI} and T_{SN} characterizing 8CB, we have obtained the value of $\zeta = 0.9375$ according to the theory of McMillan.[18] Needless to say that at temperatures above $T_{SN} = 33.5$ °C only the nematic order survives and the curves display only the lower branch of the solid line.

The results of these calculations together with the theoretical formalism described in section 2 lead to the solid lines in the phase diagrams given below.

(b) Phase Diagrams. Figure 2a,b,c shows the phase diagrams for the three systems under investigation with $M_w = 4 \times 10^3$, 44×10^3, and 200×10^3 g/mol, respectively. Each of the three phase diagrams were established on the basis of data recorded on two independently prepared samples with practically the same composition. This enables one to double check the validity of the measured data. The symbols represent the experimental results as indicated on the figure captions, and the solid lines are the theoretical predictions. The parameters used to plot these lines are chosen to reach the best fit to data. The three diagrams show an upper critical solution temperature shape. Unlike Figure 2a, the other two have a distinct critical point and an (I + I) biphasic region. The temperature and composition at the critical point increase with the molecular weight according to the mean field theory prediction. The number of adjusted parameters to fit experimental data is reduced in the presence of the critical point because the number of repeat units of the polymer N_2 is calculated from the critical volume fraction for each of the two highest molecular weight systems using $\varphi_c = N_2^{1/2}/[N_1^{1/2} + N_2^{1/2}]$, assuming that $N_1 = 1$. These values are given in the figure caption. Knowing N_1 and N_2, one can determine the critical interaction parameter using $\chi_c = [N_1^{-1/2} + N_2^{-1/2}]^2/2$. Only one parameter remains to fit the data. Therefore, values are given to A, and B is deduced according to $B = [\chi_c\text{-}A]T_c$. This procedure was possible in Figure 2b,c, whereas in Figure 2a, the absence of the critical point makes the choice of fitting parameters more arbitrary. Nevertheless, good agreement is reached between the three sets of experimental data obtained from POM, LS, and DSC, and theoretical predictions. The variations of the χ-parameter with temperature for the three systems chosen to plot the theoretical curves are given in the figure caption.

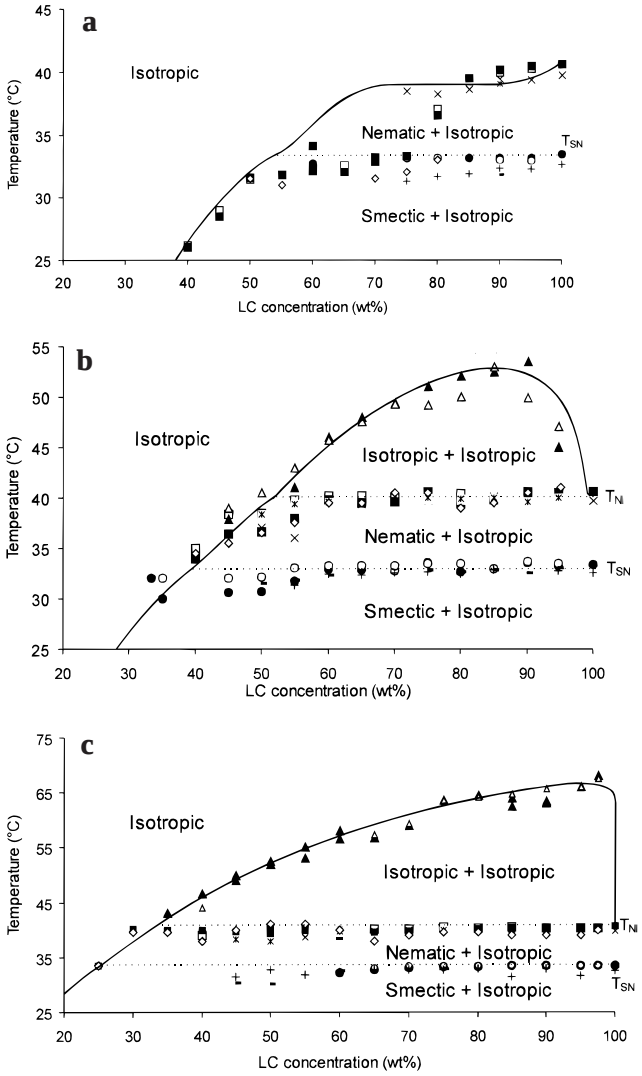

Figure 2. Equilibrium phase diagrams of PS/8CB. The symbols in this diagram represent experimental data obtained by POM and DSC: ○ and ● represent the transition temperature from smectic A+isotropic to nematic+isotropic for the two series of samples by POM measurements; □ and ■ represent the transition temperature from nematic+isotropic to isotropic+isotropic for the two series of samples by POM measurements; △ and ▲ represent the transition temperature from isotropic+isotropic to isotropic for the two series of samples by POM measurements; + and − represent the transition temperature from smectic A+isotropic to nematic+isotropic for the two series of samples by DSC measurements; *x* and * represent the transition temperature from nematic+isotropic to isotropic+isotropic for the two series of samples by DSC measurements; and ◇ represent the transition temperature from nematic+isotropic to isotropic+isotropic or isotropic obtained by LS measurements. (a) $M_w = 4 \times 10^3$ g/mol. (b) $M_w = 44 \times 10^3$ g/mol. (c) $M_w = 200 \times 10^3$ g/mol. The solid curves represent the theoretical predictions obtained using the following parameters: $T_{SN} = 33.5$ °C, $T_{NI} = 40.5$ °C, $\zeta = 0.9375$, and (a) $\chi = -0.93 + 531.3/T$, $N_2 = 15$; b) $\chi = -2.408 + 1010.76/T$, $N_2 = 32$; and (c) $\chi = -4.558 + 1733.14/T$, $N_2 = 361$.

The diagrams exhibit several regions with a distinct difference between the lowest polymer molecular weight (Figure 2a) and the other two (Figure 2b,c). Mixtures with the short polymer chain do not exhibit the biphasic region of coexisting isotropic phases as are shown in the other cases. This is due to the higher compatibility between the short polymer and the LC as compared to that with the long polymers. The enhanced compatibility

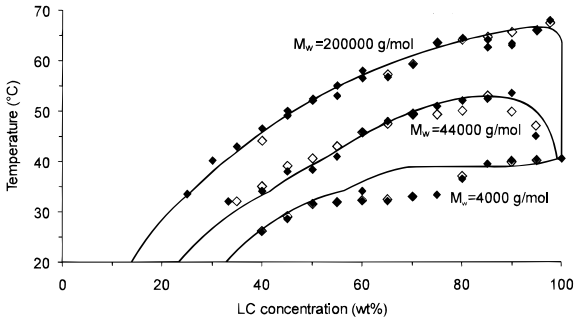

Figure 3. Transition temperatures to the isotropic phase for the three systems in the descending order from the top: $M_w = 200 \times 10^3$, 44×10^3, and 4×10^3 g/mol. The symbols ◇ and ◆ represent experimental data obtained by POM, LS, and DSC, and the solid lines are theoretical predictions calculated with the parameters given in the caption of Figure 2.

results in a direct transition from the (N + I) region to the homogeneous isotropic phase as soon as the temperature of the nematic−isotropic transition is crossed. The system with highest M_w presents the largest miscibility gap, which covers a range of temperature up to the critical temperature 65 °C, and a domain of composition from approximately 15 to 100 wt % LC, as shown in Figure 2c. The transition from smectic to nematic order is observed for the three systems at approximately the same temperature. There is a tendency toward a decrease of this transition appearing for lower LC compositions. This perturbation is probably due to the influence of T_g, which is quite close to this region. Apart from this effect, the temperature at which the transition from (S + I) to (N + I) takes place is independent of the molecular weight and is the same as that for pure 8CB, namely, $T_{SN} = 33.5$ °C. This can easily be understood by noting that in the regions (S + I) and (N + I) a polymer-rich phase dissolving the LC in the isotropic state is in equilibrium with the almost pure LC phase either in the smectic order (lower region S + I) or in the nematic order (upper region N + I). Hence, it is reasonable to expect that the transition temperature from S- to N-order of the LC remains practically constant at 33 °C, characterizing pure 8CB regardless of the amount of polymer in the sample, provided that this amount is sufficient to form an ordered phase. Melting down of the nematic order into an isotropic phase takes place roughly at 40.5 °C, characteristic of the (N−I) transition of the pure LC for the three systems investigated here. The explanation is the same as that above in the transition from smectic to nematic order.

To illustrate further the effect of polymer size on the phase behavior of the three systems, we reproduce in Figure 3, the change in the highest transition temperature with composition only. The upper curve represents the highest molecular weight and shows a transition from an (I + I) to an I region, whereas for the lower curve corresponding to the lowest M_w, one has a direct transition from an (N + I) region to a single isotropic phase. A drastic loss of miscibility follows an increase of polymer size. Consequently, the amount of LC dissolved in the polymer matrix decreases substantially. Quantification of these tendencies has an important impact upon quality of these systems in practical applications. They represent valuable guides for the choice of adequate materials suitable for some applications.

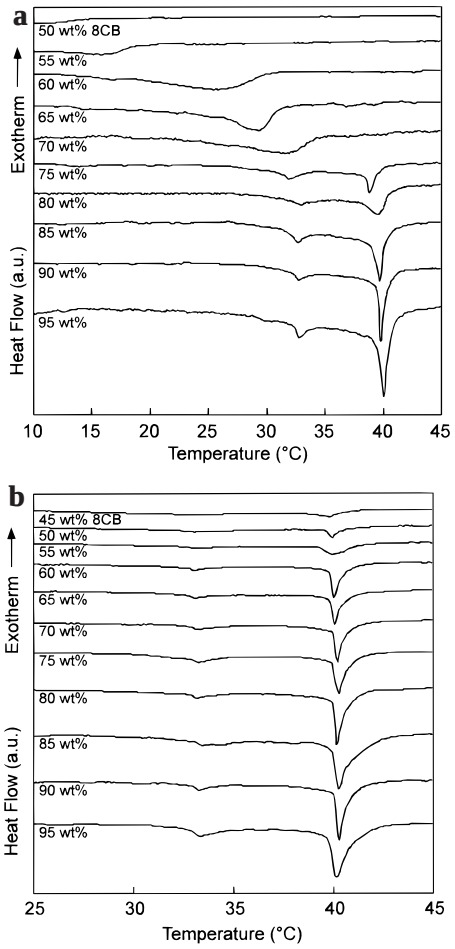

Figure 4. (a) DSC thermograms of the PS/8CB mixture with $M_w = 4 \times 10^3$ g/mol of compositions from 50 to 95 wt % 8CB recorded during the second heating at a rate of 2 °C/min. (b) Same as that in part a for $M_w = 200 \times 10^3$ g/mol recorded under similar conditions in a composition range from 45 to 95 wt % 8CB.

Optical micrographs showing coexisting domains of smectic-A order with isotropic phases and nematic domains with isotropic phases were given in Benmouna et al.[14] for the system with intermediate molecular weight of PS. Similar textures were obtained for the other systems with minor differences. For example, the ordered domains observed in the system with lowest M_w are less developed and more difficult to identify due to the higher compatibility of the LC and the polymer. The higher molecular weight polymer systems exhibit much larger and more defined ordered domains.

To improve understanding of the thermal properties of these systems, it is useful to analyze with further details the energetic data obtained by DSC measurements that is the subject of the following section.

4.2. Thermophysical Properties. *(a) DSC Data.* Parts a and b of Figure 4 display the thermograms corresponding to mixtures with PS molecular weight $M_w = 4 \times 10^3$ and 200×10^3 g/mol, respectively, and the LC composition from 45 to 95 wt % 8CB. The thermograms for $M_w = 44 \times 10^3$ g/mol were given in Benmouna et al.[14] and are not reproduced here. Measurements made for the system with $M_w = 44 \times 10^3$ g/mol up to 30 wt % 8CB revealed a plasticizing effect of the LC for PS via a sharp decrease of the glass-transition temperature T_g from 103 °C for pure PS down to about 17 °C for 30 wt % LC. For this system, up to 30 wt % 8CB,

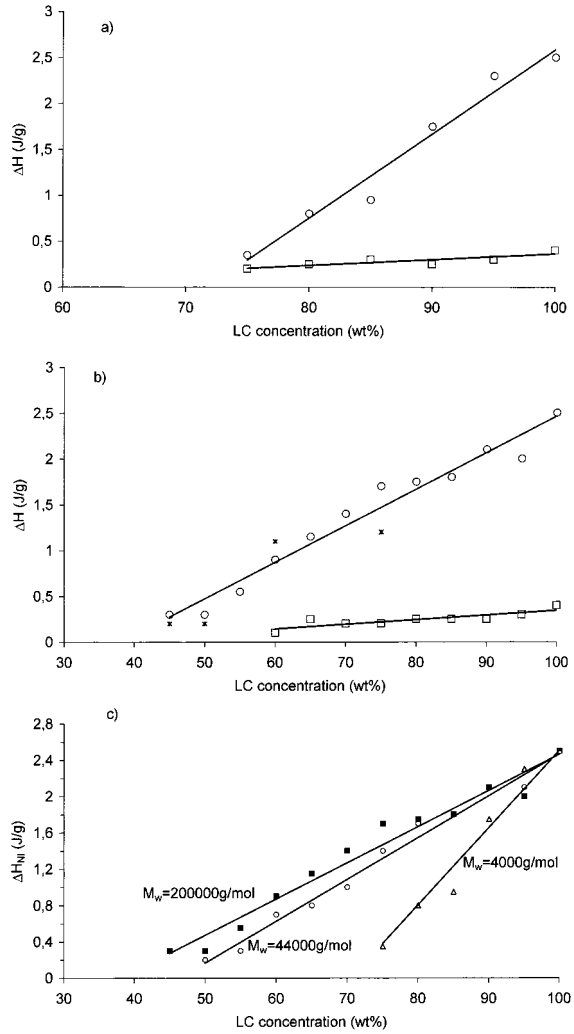

Figure 5. Enthalpy variations in the nematic−isotropic transition ΔH_{NI} and the smectic A−nematic transition, ΔH_{SN}, versus 8CB concentration. (a) $M_w = 4 \times 10^3$g/mol, (b) $M_w = 200 \times 10^3$g/mol, and (c) only ΔH_{NI} versus LC concentration for the three molecular weights. The symbols ■, ○, and △ represent the ΔH_{NI} data for the three systems in the descending order of M_w. *x* correspond to data obtained independently from a second series of samples of $M_w = 200 \times 10^3$g/mol. The symbol □ represents data of ΔH_{SN}.

there is complete miscibility of PS and 8CB. The DSC thermograms exhibit a single glass transition, and the sample remains isotropic at all temperatures covered in the experiments. For the PS of highest molecular weight, the range of miscibility shrinks substantially, and a gap appears at less than 15 wt % 8CB for $T = 20$ °C, for example.

(b) Enthalpy Data. Parts a and b of Figure 5represent enthalpy changes at the (S + N) and (N + I) transitions versus composition for the mixtures with lowest and highest molecular weights, respectively. Enthalpy changes in the (N + I) transition are larger that in the (S + N) transition. The energy cost to align randomly oriented LC molecules to form a nematic phase is much higher than to rearrange the oriented molecules and achieve a smectic-A order. This is true for the three systems considered here. The results for the intermediate molecular weight are not reproduced here and can be found in Benmouna et al.[14] Measurements of enthalpy changes in the (N + I) transition are much more precise than those of the (S + N) transition, which shows

scattered data. Observations made from the ΔH_{NI} data are more reliable, and therefore, we shall proceed with the discussion of thermophysical properties extracted from the (N + I) energy data only.

To allow comparison of the results obtained for different molecular weights, we present in Figure 5c ΔH_{NI} versus $\varphi_{LC} = \varphi_1$ for the three systems investigated. One observes that ΔH_{NI} increases linearly with LC content and the three curves merge together at $\varphi_1 = 1$ to the same value, namely, 2.6 J/g. The increase of ΔH_{NI} is steeper for lower molecular weight as the concentration of LC increases.

(c) Solubility Data. The above thermal data enable one to extract the solubility limit β of the LC in the polymer, which gives a direct estimate of the relative amount of LC in nematic domains. Let δ be the ratio of enthalpy changes at the (N + I) transition for the mixture at composition φ_1 and for the bulk LC

$$\delta = \Delta H_{NI}(\varphi_1)/\Delta H_{NI}(\varphi_1=1) \tag{25}$$

The rule of inverse segments yields a relationship between δ and the solubility limit β as

$$\delta = (\varphi_1 - \beta)/(1 - \beta) \tag{26}$$

where $\varphi_1 > \beta$, otherwise $\delta = 0$. This assumes that the LCs inside nematic domains and in the pure state have similar thermophysical properties and that the polymer dissolved in the LC phase does not contribute to the enthalpy change $\Delta H_{NI}(\varphi_1)$. Moreover, the (N + I) transition temperature is assumed to remain constant upon addition of polymer.

Figure 5c shows that $\Delta H_{NI}(\varphi_1)$ increases linearly with φ_1 consistent with eq 26 and literature data.[5,6,8,9,29,30] The intercepts of the lines with the *x*-axis yield the solubility limit β and decrease strongly with increasing molecular weight of the polymer. One reads $\beta = 0.37$, 0.47, and 0.71 in the decreasing order of PS molecular weight. It is interesting to note that for the systems investigated by Smith,[5] which usually involve chemically cross-linked networks, the typical values of β vary from 0.1 to 0.2. In view of these remarks, we see that the present values of β are comparatively high. On the other hand, the fraction of 8CB contained in the nematic domain α is another interesting quantity. It is given by the ratio of the mass of LC in the nematic domain m_1^D and that of the LC in the whole mixture m_1

$$\alpha = m_1^D/m_1 = \delta/\varphi_1 \tag{27}$$

Figure 6 shows α versus φ_1 for the three systems under investigation. Clearly, similar information is contained in the curves of ΔH_{NI} versus φ_1 (Figure 5), but Figure 6 has the merit of giving directly the amount of LC in the nematic domains and shows how this amount increases with the polymer size. These plots show that α can be quite large if the polymer size increases. In the case of a low-molecular-weight polymer, α could roughly be described by a linear segment, but as the polymer size increases, the data show that α first increases and then tends to level off as the concentration of LC becomes high. For a large polymer, there is a strong increase in α below $\varphi_1 = 0.7$. Above this concentration, the value of α remains approximately constant, indicating saturation of the polymer-rich phase. This tendency is also seen for the intermediately sized polymer, but the concentration of LC where saturation is reached is higher.

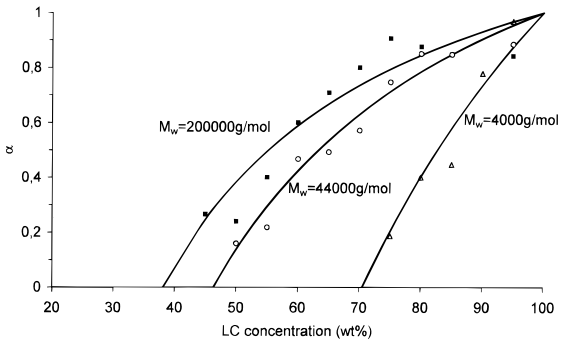

Figure 6. Fraction of 8CB in nematic droplets α obtained from ΔH_{NI} data versus total LC composition for the three molecular weights in the decreasing order from the top. The symbols ■, ○, and △ represent the data for the three systems in the decreasing order of molecular weight determined by applying eq 27, whereas the solid lines were calculated by using the corresponding β values from Figure 5c and eq 26.

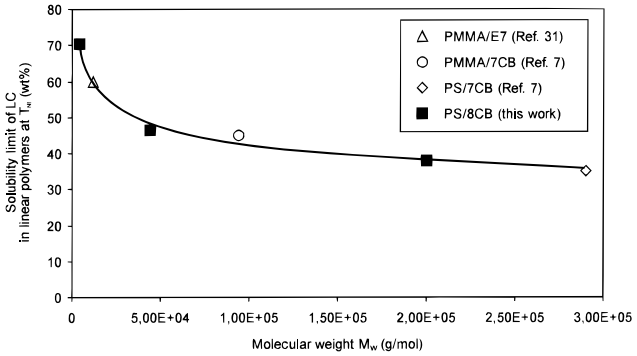

Figure 7. Experimental data showing the variation of α as a function of polymer molecular weight for different linear polymer/LC mixtures. The data shown here include results of the present work and results taken from the literature as indicated on the figure. The solid line is a least-squares fit to the data.

Figure 7 represents the variation of the solubility limit of the LC at T_{NI} with the polymer molecular weight. This plot includes data of the present work and other data published in the literature for other mixtures of linear polymers and low-molecular-weight LC.[7,31] Although these systems involve different polymers and different LC, the results fall on the same master curve. Beyond a certain polymer size, the solubility of the LC in the polymer reaches a plateau limit. If such a variation is confirmed, then this result would allow prediction of the solubility limit of other systems. This could have important consequences because it would mean that beyond a certain polymer molecular weight the nature of the species in the mixture is irrelevant as long as α is concerned.

5. Conclusions

The phase behavior of PS/8CB mixtures with three molecular weights of the polymer differing by 2 orders of magnitude is studied both experimentally and theoretically. The experimental data are obtained using POM, LS, and DSC and allow construction of the complete phase diagrams for the three systems. These diagrams exhibit several regions: At low temperatures, a miscibility gap consisting of an isotropic polymer-rich phase coexisting with a smectic LC phase is observed

for all molecular weights. At temperatures above 33.5 °C, there is a transition from smectic to nematic order, and one obtains an (N + I) biphasic region for the three systems. Above 40.5 °C, the LC in the ordered phase becomes isotropic, but the transition depends strongly on the polymer size. For the two highest molecular weights, the phase diagrams show an (I + I) miscibility gap, whereas for the lowest molecular weight, a direct transition from a (N + I) to a single isotropic I phase is found. Clearly, the latter system exhibits a much higher solubility of the LC in the polymer than those of the other systems considered here. This enhanced compatibility is expressed not only by the absence of an (I + I) gap but also by a significant shift of the cloud point curve to the right, leaving a much wider region for the single I phase.

The experimental phase diagrams are analyzed with the theoretical framework combining the Flory−Huggins theory of isotropic mixing and the Maier−Saupe theory of nematic order generalized by McMillan to include smectic-A order. Good agreement is obtained between experimental data and theoretical predictions.

In addition to phase diagrams, the thermophysical properties obtained from DSC measurements were analyzed according to the procedure suggested by Smith.[29,30] Both enthalpy changes in the (S−N) and (N−I) transitions were examined to deduce solubility limits of the LC in the polymer. The data for ΔH_{SN} are not sufficiently accurate to allow for reliable predictions of the solubility properties. However, the enthalpy changes in the (N−I) transitions are much more significant and were used successfully to obtain with good accuracy the solubility limits and the amount of LC dissolved in the polymer. In particular, the effect of polymer molecular weight on these thermal properties were unambiguously identified via a miscibility loss with increasing molecular weight. A single curve representing the solubility limit versus polymer molecular weight for several systems is obtained. This result allows one to make predictions on other systems with different polymers and LCs without having to make additional measurements. The curve of the solubility limit at T_{NI} versus molecular weight shows a sharp decrease for relatively low M_w followed by a leveling-off indicating saturation of the polymer-rich phase. This phenomenon might be related to the formation of a physical network due to a strong entanglement of polymer chains as the molecular weight increases. To our knowledge, this is the first time that such observations are made on the variation of the solubility limit of polymer/LC mixtures with the size of the polymer. It is evident that further studies will be necessary to understand the relationship between the solubility limit of the LC and the polymer molecular weight.

Acknowledgment. This work has been accomplished during a stay of F.B. at the "Université du Littoral" (Dunkerque, France) as a guest professor.

References and Notes

(1) Doane, J. W. Polymer Dispersed Liquid Crystal Displays. In *Liquid Crystals: Their Applications and Uses*; Bahadur, B., Ed.; World Scientific: Singapore, 1990.
(2) Drzaic, P. S. *Liquid Crystal Dispersions*; World Scientific: Singapore, 1995.
(3) *Liquid Crystals in Complex Geometries*; Crawford, G P., Zumer, S., Eds.; Taylor & Francis: London, 1996.
(4) Maschke, U.; Coqueret, X.; Loucheux, C. *J. Appl. Polym. Sci.* **1995**, *56*, 1547.
(5) Smith, G. W. *Mol. Cryst. Liq. Cryst.* **1990**, *180B*, 201.
(6) Russell, G. M.; Paterson, B. J. A.; Imrie, C. T.; Heeks, S. K. *Chem. Mater.* **1995**, *7*, 2185.
(7) Ahn, W.; Kim, C. Y.; Kim, H.; Kim, S. C. *Macromolecules* **1992**, *25*, 5002.
(8) Maschke, U.; Roussel, F.; Buisine, J.-M.; Coqueret, X. *J. Therm. Anal.* **1998**, *51*, 737.
(9) Roussel, F.; Buisine, J.-M.; Maschke, U.; Coqueret, X. *Mol. Cryst. Liq. Cryst.* **1997**, *299*, 321.
(10) Maschke, U.; Turgis, J.-D.; Traisnel, A.; Coqueret, X. *Mol. Cryst. Liq. Cryst.* **1996**, *282*, 407.
(11) Gyselinck, F.; Maschke, U.; Traisnel, A.; Coqueret, X. *Mol. Cryst. Liq. Cryst.* **1999**, *329*, 569.
(12) Kyu, T.; Shen, C.; Chiu, H.-W. *Mol. Cryst. Liq. Cryst.* **1996**, *287*, 27.
(13) Kim, W.-K.; Kyu, T. *Mol. Cryst. Liq. Cryst.* **1994**, *250*, 131.
(14) Benmouna, F.; Daoudi, A.; Roussel, F.; Buisine, J.-M.; Coqueret, X.; Maschke, U. *J. Polym. Sci., Part B: Polym. Phys.* **1999**, *37*, 1841.
(15) Flory, P. J. *Principles of Polymer Chemistry*; Cornell University Press: Ithaca, NY, 1965.
(16) Maier, W.; Saupe, A. *Z. Naturforsch.* **1959**, *14A*, 882.
(17) Maier, W.; Saupe, A. *Z. Naturforsch.* **1960**, *15A*, 287.
(18) McMillan, W. L. *Phys. Rev. A* **1971**, *4*, 1238.
(19) De Gennes, P. G.; Prost, J. *The Physics of Liquid Crystals*; Oxford Science Publications: Oxford, U.K., 1994.
(20) Chandrasekhar, S. *Liquid Crystals*, 2nd ed.; Cambridge University Press: Cambridge, U.K., 1992.
(21) Gray, G. W.; Goodby, J. W. *Smectic Liquid Crystals: Textures and Structures*; Leonard Hill, Heyden & Son Inc.: Philadelphia, 1984.
(22) Kyu, T.; Chiu, H.-W. *Phys. Rev. E* **1996**, *53*, 3618.
(23) Chiu, H.-W.; Kyu, T. *J. Chem. Phys.* **1997**, *107*, 6859.
(24) Chiu, H.-W.; Kyu, T. *J. Chem. Phys.* **1998**, *108*, 3249.
(25) Kyu, T.; Liang, S.; Chiu, H.-W. *Macromolecules* **1998**, *31*, 3604.
(26) Matsuyama, A.; Kato, T. *J. Chem. Phys.* **1998**, *108*, 2067.
(27) Benmouna, F.; Coqueret, X.; Maschke, U.; Benmouna, M. *Macromolecules* **1998**, *31*, 4879.
(28) Leclercq, L.; Maschke, U.; Ewen, B.; Coqueret, X.; Mechernene, L.; Benmouna, M. *Liq. Cryst.* **1999**, *26*, 415.
(29) Smith, G. W.; Vaz, N. A. *Liq. Cryst.* **1988**, *3*, 543.
(30) Smith, G. W.; Ventouris, G. M.; West, J. L. *Mol. Cryst. Liq. Cryst.* **1992**, *213*, 11.
(31) Challa, S. R.; Wang, S. Q.; Koenig, J. L. *J. Therm. Anal. Cal.* **1995**, *45*, 1297.

MA991228D